NANO LETTERS

pubs.acs.org/NanoLett Letter

Data-Driven Quest for Two-Dimensional Non-van der Waals Materials

Rico Friedrich,* Mahdi Ghorbani-Asl, Stefano Curtarolo, and Arkady V. Krasheninnikov

Cite This: *Nano Lett.* 2022, 22, 989–997 Read Online

ACCESS | Metrics & More | Article Recommendations | Supporting Information

ABSTRACT: Two-dimensional (2D) materials are frequently associated with the sheets forming bulk layered compounds bonded by van der Waals (vdW) forces. The anisotropy and weak interaction between the sheets have also been the main criteria in the computational search for new 2D systems, predicting ~2000 exfoliable compounds. However, some representatives of a new type of non-vdW 2D systems, without layered 3D analogues, were recently manufactured. For this novel materials class, data-driven design principles are still missing. Here, we outline a set of 8 binary and 20 ternary candidates by filtering the AFLOW-ICSD database according to structural prototypes. The oxidation state of the surface cations regulates the exfoliation energy with low oxidation numbers leading to weak bonding—a useful descriptor to obtain novel 2D materials also providing clear guidelines for experiments. A vast range of appealing electronic, optical, and magnetic properties make the candidates attractive for various applications and particularly spintronics.

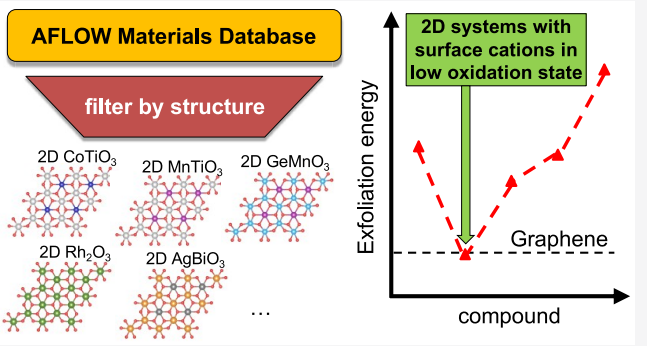

KEYWORDS: *2D materials, exfoliation, data-driven research, computational materials science, high-throughput computing*

Downloaded via HELMHOLTZ ZENTRUM on February 9, 2022 at 10:13:51 (UTC).
See https://pubs.acs.org/sharingguidelines for options on how to legitimately share published articles.

The isolation of single graphene sheets,[1] which proved that two-dimensional (2D) systems can exist, gave rise to the discovery of many 2D materials with unique superconducting,[2,3] electronic,[4−6] magnetic,[7−9] and topological[10] properties. In addition to being testbeds for studying the behavior of systems in reduced dimensions, 2D materials hold great promise for various applications in optoelectronics,[4,11,12] catalysis,[13,14] and the energy sector.[15−17] The research effort has been mainly concentrated on the systems which have bulk counterparts representing anisotropic crystals with layers held together by van der Waals (vdW) forces, with the most prominent example being graphene and graphite. The weak interlayer interaction leads to a natural structural separation of the 2D subunits in the crystals, therefore making the mechanical[18] or liquid-phase[19] exfoliation possible.

At the same time, the layered structure allows developing rigorous screening criteria for exfoliability to be employed on large materials databases—outlining data-driven high-throughput investigations as an ideal tool for the discovery and design of 2D compounds.[20−28] Such studies predicted several thousands of vdW 2D systems and were used to set up computational databases.[21−23,25,26]

Unexpectedly, a new direction in the research on 2D systems was opened in 2018, after the experimental realization of atomically thin sheets from non-vdW bonded compounds by a special chemical exfoliation process.[29,30] The first representatives of these non-vdW 2D materials were hematene and ilmenene obtained from the earth-abundant ores hematite (α-Fe_2O_3) and ilmenite ($FeTiO_3$), followed by other systems derived from chromite ($FeCr_2O_4$),[31] magnetite (Fe_3O_4),[32] pyrite (FeS_2),[33,34] chromium sulfide,[35] manganese selenide (α-$MnSe_2$),[36] metal diborides,[37] boro-carbides,[38] and diamond-like germanium (α-Ge).[39]

While traditional vdW compounds have chemically saturated bonds at the surface of 2D subunits, the aforementioned materials show qualitatively new features. As they are obtained from nonlayered systems, they exhibit dangling bonds and surface states, making them more tunable by adsorbates.[40] They have already shown great potential for electronic[41] and optoelectronic[42] applications and by exhibiting enhanced photocatalytic activity for water splitting[29,30] and photoconductivity.[36] Moreover, they may also offer a versatile playground for magnetism and spintronics in reduced dimensions.[43] The first studies mostly focusing on hematene indicate, for instance, tunable magnetic ordering,[29,30,40,44−47] as well as spin canting.[48]

Although there have been significant experimental efforts to generalize recipes for their synthesis,[37,38,41,47,50] computational

Received: October 5, 2021
Revised: January 5, 2022
Published: January 20, 2022

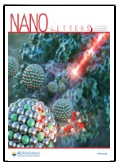

© 2022 The Authors. Published by American Chemical Society

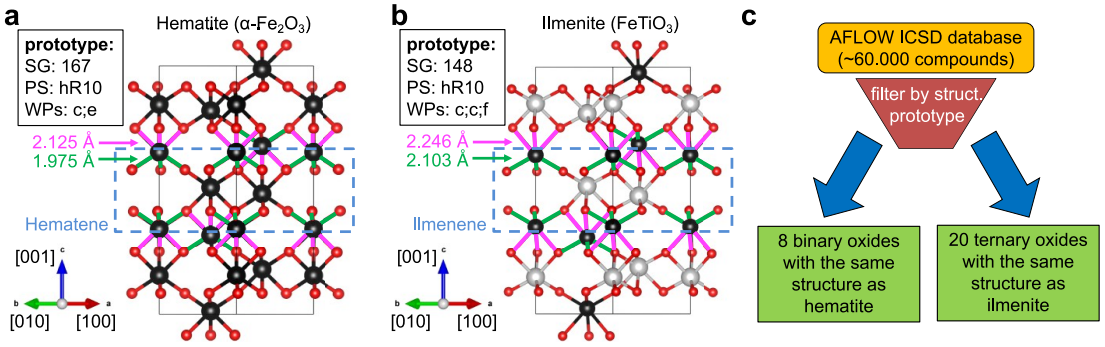

Figure 1. Structural prototypes of non-vdW 2D materials. Atomic structures of (a) hematite (α-Fe_2O_3) and (b) ilmenite ($FeTiO_3$), the first non-vdW bulk materials with 2D analogues.[29,30] Long (weak) bonds are highlighted in magenta, and short (strong) bonds are indicated in green as obtained from PBE+*U*. For both prototypes, space groups (SGs), Pearson symbols (PSs), and Wyckoff positions (WPs) are indicated in the respective boxes. In each case, the exfoliable [001] facet (monolayer) is indicated in the blue dashed frame leading to hematene and ilmenene 2D materials. Colors: Fe, black; O, red; and Ti, light gray.[49] The black line denotes the conventional unit cell. (c) Schematic workflow illustrating how the candidate systems were obtained from the AFLOW ICSD database using structural information as an input.

design principles based on data-driven concepts for outlining non-vdW 2D materials are still missing. It is obvious that the descriptors developed for vdW-bonded systems are not applicable, since they rely on identifying layered subunits in the structure.

Here, we resolve this issue by screening the AFLOW database[51] using the structure of the previously realized representatives as an input and identify 28 non-vdW potentially synthesizable 2D materials. We further show that they exhibit a vast range of promising electronic, optical, and magnetic properties, suggesting in particular spintronic applications. The oxidation state of the cations at the surface of the 2D slab is outlined as a key quantity determining the easy exfoliation of the systems, thus providing an enabling descriptor for the discovery of novel 2D materials.

OUTLINING MORE CANDIDATES

Hematite and ilmenite, Figure 1a,b—the first non-vdW materials with 2D analogous[29,30]—can be used as a template for screening the AFLOW-ICSD database containing ~60 000 compounds, Figure 1c. This library primarily incorporates materials realized experimentally. When closely investigating the structure of the hematite and ilmenite prototypes, one recognizes that the Fe−O bond lengths are strongly anisotropic. As indicated in Figure 1a, for hematite, there are three long (weak) bonds of 2.125 Å and three shorter (stronger) ones of 1.975 Å highlighted in magenta and green, respectively, for each Fe close to the exfoliation planes. When slicing the structure between the Fe cations as indicated by the blue dashed lines, one only cuts through the weak (long) bonds. For any other surface termination, one would need to break stronger bonds. For $FeTiO_3$, the situation is similar exhibiting Fe−O bonds of 2.246 and 2.103 Å (see Figure 1b). We believe that this natural separation of the bond strengths together with electrostatic considerations is key to the exfoliability of these materials. It is a characteristic of the outlined prototypes and thus reveals their particular suitability for the emergence of non-vdW 2D systems. (The Ti−O bond lengths in $FeTiO_3$ are also anisotropic amounting to 1.944 and 2.078 Å. Ti is, however, not the terminating ion at the surface of ilmenene as found consistently by experiment[30] and calculations. This is related to its higher oxidation state (Ti^{4+} vs Fe^{2+}), making this configuration energetically unfavorable as discussed in detail in the text below.) We thus look for other systems with the same structural prototype.[52,53] Two structures are regarded to have the same prototype if their space group (SG), Pearson symbol (PS), and Wyckoff positions (WPs) match, which are indicated for α-Fe_2O_3 (corundum) and $FeTiO_3$ in Figure 1.

The search yields the 8 binary and 20 ternary oxides (excluding P, As, and Sb, as these are not typical cation species) listed in Table 1. (Structural data are retrieved via the AFLOW APIs[54,55] and web interfaces[51] as well as the library of crystallographic prototypes.[56]) We decided to focus on oxides since these are abundant materials and typically of high interest for technological applications. For each composition, the listed frequency of occurrence in the database (in brackets after the formula) gives a first indication how common the system is. These candidates are now investigated for the formation of the corresponding 2D sheets perpendicular to the [001] direction (called [001] facets) in analogy to the template systems. This facet has been outlined as thermodynamically favorable for hematene.[29,40] Here, the monolayer structures according to refs 29 and 30 and Figure 1a,b are considered, which are referred to as 2D systems in the following. This limit provides

Table 1. Binary and Ternary Compositions with the Same Structures as Hematite and Ilmenite[a]

binaries		ternaries			
composition	mag.	composition	mag.	composition	mag.
Al_2O_3 (72)	no	$MgTiO_3$ (28)	no	$CaSnO_3$ (1)	no
Fe_2O_3 (63)	yes	$FeTiO_3$ (21)	yes	$CdGeO_3$ (1)	no
Cr_2O_3 (52)	yes	$GeMgO_3$ (7)	no	$CdTiO_3$ (1)	no
V_2O_3 (20)	yes	$MgSiO_3$ (7)	no	$CoMnO_3$ (1)	yes
Ti_2O_3 (15)	yes	$GeMnO_3$ (6)	yes	$CuVO_3$ (1)	no
Rh_2O_3 (4)	no	$MnTiO_3$ (5)	yes	$GeZnO_3$ (1)	no
Ga_2O_3 (3)	no	$NiTiO_3$ (5)	yes	$MnNiO_3$ (1)	yes
In_2O_3 (3)	no	$AgBiO_3$ (2)	no	$SiZnO_3$ (1)	no
		$BiNaO_3$ (2)	no	$SnZnO_3$ (1)	no
		$CoTiO_3$ (2)	yes	$TiZnO_3$ (1)	no

[a]Binary compositions with the same structural prototype as hematite (α-Fe_2O_3) and ternary compositions with the same structural prototype as ilmenite ($FeTiO_3$) from the AFLOW- ICSD database. The numbers in brackets after the compound formulas of each system indicate the frequency of occurence in the database. Whether the structure was found to exhibit magnetic moments is also indicated.

https://doi.org/10.1021/acs.nanolett.1c03841
Nano Lett. 2022, 22, 989−997

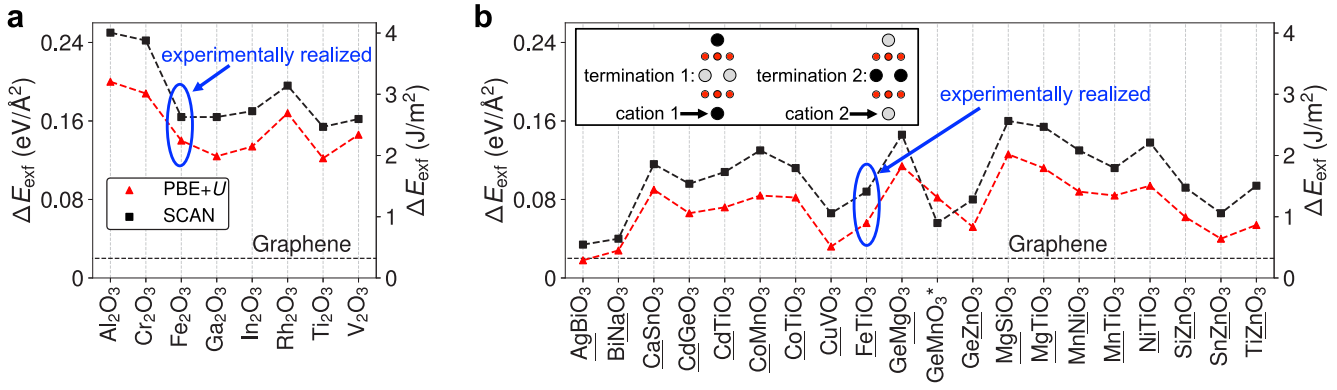

Figure 2. Exfoliation energies. Exfoliation energies of investigated (a) binary and (b) ternary systems for two different functionals. As a reference, the exfoliation energy of graphene[25,58] is indicated by the dashed horizontal black lines. For the ternaries, the data for the slabs with the energetically favorable termination are plotted, and the terminating element is underlined at the bottom axis. The inset indicates the two possible terminations. In the case of $GeMnO_3$ (marked by "*"), PBE+*U* favors Mn termination, while for SCAN Ge termination is preferred. Note that, for Al_2O_3, $BiNaO_3$, $GeMgO_3$, and $MgSiO_3$, PBE+*U* reduces to plain PBE. Data points for 2D systems realized experimentally[29,30] are highlighted. The dashed lines connecting the data points are visual guides.

an upper energetic bound to obtain 2D sheets from a given material.[40]

A recent study in ref 57 demonstrated that the relation between the in-plane tearing energy and the out-of-plane peeling energy controls the length to thickness aspect ratio of liquid-exfoliated nanosheets, implying that layered materials with large mechanical anisotropy prefer to yield nanosheets with large aspect ratios. Similarly, one can expect that nonlayered materials with anisotropic bonding schemes can also be exfoliated into nonlayered quasi-2D materials according to this assessment.[33,38] Such an exfoliation process might also lead to surface passivation due to the liquid environment.[32]

EXFOLIATION ENERGIES

The exfoliation energies ΔE_{exf} are computed as the energy difference between relaxed 2D and bulk systems in accordance with ref 59. This work demonstrated the strict equivalence of the binding energy between facets/layers in the bulk and the exfoliation energy from the surface of the material. The results are presented in Figure 2. They were obtained by relaxing both the ionic positions and the cell shape of the 2D sheets. In Figures S1 and S2, a comparison of the calculated exfoliation energies also including results from different functionals as well as from relaxing different degrees of freedom of the systems is presented showing that these 2D materials primarily gain energy due to the ionic relaxation (see also the paragraphs on structural properties below). For vdW bonded compounds, relaxations of 2D substructures could be omitted when calculating inter-*layer* binding energies,[25] which is, however, not a good approximation for the present non-vdW systems. Note that, for the ternaries (Figure 2b), either of the two cation species can be at the surface of the 2D slabs. The graph includes the results for the energetically more stable termination, and the respective terminating element is underlined at the bottom axis. A plot comparing the exfoliation energies obtained with the different terminations is given in Figure S3.

The values are presented for the two DFT methodologies, PBE+*U* and SCAN. The former is a standard approach for transition metal based systems, which has been used in several previous studies on hematene.[29,40,44] The latter is a more sophisticated method, which has been demonstrated to provide accurate structures and energies for diversely bonded systems.[60] Both approximations show similar trends and magnitudes of the exfoliation energy with SCAN generally giving higher values. As a reference, the ΔE_{exf} of graphene—well-known to be exfoliable—which is found to be ∼20 meV/Å^2 by both theory and experiment,[25,58,61] is also indicated. While for all binary systems in Figure 2a the exfoliation energy is considerably higher than for graphene, the value of 140 meV/Å^2 computed for hematene with PBE+*U* nicely fits to previously reported values (after accounting for the different normalization by a factor of 2),[40,44] employing slightly different computational parameters. Considering that hematene has been realized experimentally, all other systems are also likely exfoliable with Al_2O_3 being a potential exception. The systems with the lowest calculated exfoliation energies are close to the limit deemed "potentially exfoliable" (upper bound for ΔE_{exf} of 130 meV/Å^2) in ref 25, albeit in this study vdW bonded materials were considered. A limit of ∼200 meV/atom for exfoliability has also been proposed,[23] which corresponds to about 2/3 of the value calculated for hematene.

As evident from Figure 2b, the ternaries show in general smaller exfoliation energies in part even close to the graphene reference, suggesting the feasibility of mechanical peel-off. Importantly, the value becomes particularly small when the element at the surface of the slab is in a low oxidation state as indicated most prominently by $AgBiO_3$, $BiNaO_3$, and $CuVO_3$, where the surface Ag, Na, and Cu are in state +1. This pattern can be understood from the fact that smaller surface charges lead to weaker Coulomb-like interactions between facets. Also Zn- and Fe-termination is energetically favorable, while Mg-termination leads to the highest ΔE_{exf} among the investigated ternaries, albeit smaller than for hematene, for which exfoliation was achieved experimentally. This general behavior has a strong effect on the magnetic properties, since it results in the magnetic ions Mn^{2+}, Fe^{2+}, Co^{2+}, and Ni^{2+} terminating the 2D materials.

In conclusion, when comparing the results for the whole set, the exfoliation energies vary by about an order of magnitude: The highest value is obtained for Al_2O_3 as 200 (250) meV/Å^2 from PBE+*U* (SCAN), whereas the lowest is calculated for $AgBiO_3$ as 18 (34) meV/Å^2. Thus, there is a pronounced difference in the (mechanical) effort to exfoliate these systems.

https://doi.org/10.1021/acs.nanolett.1c03841
Nano Lett. 2022, 22, 989−997

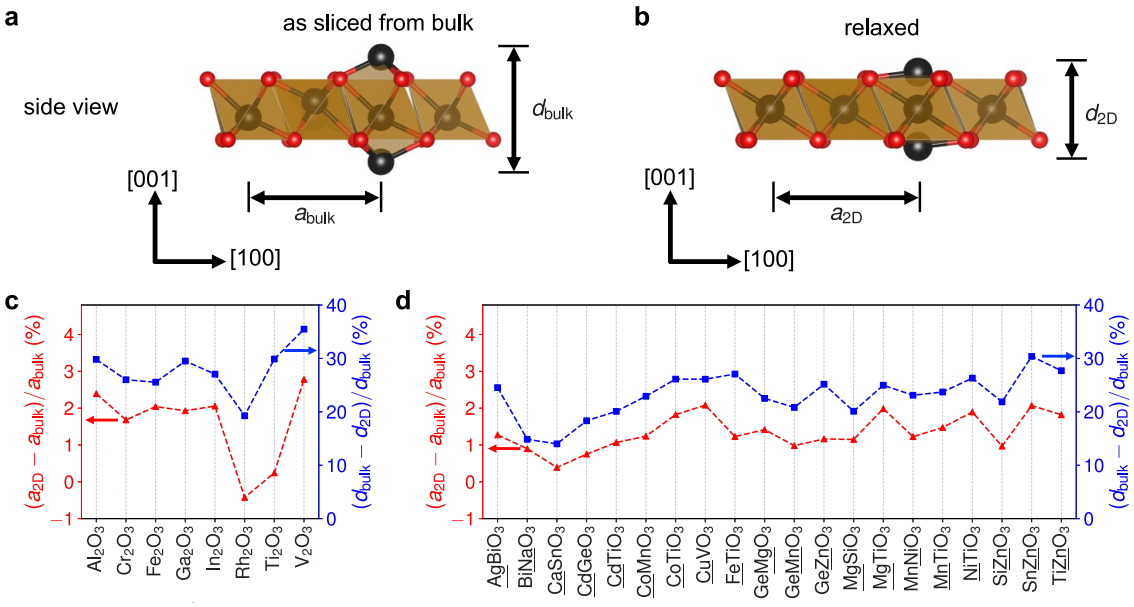

Figure 3. Modification of structural parameters. Side views of the (a) initial and (b) relaxed unit cells of [001] hematene. Fe coordination polyhedra are visualized in brown. Change of structural parameters for (c) binary and (d) ternary non-vdW materials upon exfoliation. The modification of the in-plane lattice parameter is indicated by the red curves (left *y*-axis), while the thickness change is given by the blue curves (right *y*-axis). The ternary data are for the energetically preferred slab termination. The dashed lines connecting the data points are visual guides.

While low surface energies for other compounds[62] might also suggest exfoliability, this is a necessary, but not sufficient, condition. The bonding between the atoms after the exfoliation and the reconstruction of the obtained sheets defining its stability is also critical. As an example, NaCl appears to have a very small surface energy[63] but is strictly unstable as a freestanding 2D system. To verify the dynamic stability of the outlined candidates in a high-throughput fashion, 2 × 2 in-plane supercells are generated from the relaxed structures with the atomic coordinates randomized (Gaussian distribution, standard deviation 50 mÅ)[64,65] and reoptimized. In each case, the systems relax back to the previously found structures, confirming their stability.

STRUCTURAL PROPERTIES

The investigated non-vdW 2D materials show pronounced structural modifications as compared to their bulk parents. In general, systems compress laterally upon confinement into 2D to compensate for the loss in the out-of-plane bonding by stronger in-plane bonds. The present compounds, however, expand. Figure 3a,b shows side views of the initial (as sliced from bulk) and relaxed structures for hematene. The in-plane lattice constants (thickness of the slab) as sliced from the bulk a_{bulk} (d_{bulk}) and for the relaxed 2D systems a_{2D} (d_{2D}) are also indicated. The relative change of a_{2D} with respect to a_{bulk} is depicted in Figure 3c,d (red curves) for PBE+*U*. An equivalent plot for SCAN showing very similar trends and magnitudes is included in Figure S4. For all systems, a strong expansion of up to ∼3% for V_2O_3 is observed. The only exception is Rh_2O_3, for which a small contraction of ∼−0.5% is found.

The expansion correlates well with a corresponding vertical contraction of the systems from d_{bulk} to d_{2D} (blue curves in Figure 3c,d), which ranges up to ∼35% for V_2O_3. The mechanism of this behavior can be understood from Figure 3a,b. In order to compensate for the dangling bonds created at the surface cations upon exfoliation, the outer atoms move toward the center of the slab during the relaxation, reducing the slab thickness. As a consequence, this exerts a stress onto the plane of oxygen anions, causing the structures to stretch laterally. For Rh_2O_3, the structure compensates for the (smaller) vertical contraction by a twist of the coordination polyhedra rather than a lateral expansion.

ELECTRONIC PROPERTIES

A detailed presentation of all band structures and densities of states is located in the Supporting Information (Figures S5 to S32), and here the main focus shall be on the band gaps. Figure 4 shows the calculated band gap energies E_{gap} for all bulk and 2D systems. While it is well-known that DFT—even in the employed PBE+*U* scheme—in general has problems predicting absolute gap values, the overall trends and differences between similar systems are often still reliable. We thus believe that the observed distribution of the gaps over a wide range (from below 1 eV to almost 6 eV) is noteworthy, pointing to the potential usefulness of these systems in, e.g., optoelectronics. For Al_2O_3, Cr_2O_3, Fe_2O_3, Rh_2O_3, and $MgSiO_3$, the 2D gap is considerably smaller than that in the bulk parent system, which can be assigned to the emergence of surface states in the gap upon exfoliation. For the other systems, however, the two gaps are similar or the trend is reversed; i.e., the 2D gap is significantly larger than the bulk one as observed for $AgBiO_3$, $FeTiO_3$, and $SnZnO_3$. This is likely associated with the strong structural relaxation described earlier. When the outer cations relax toward the planes of oxygen anions, Figure 3a,b, the electronic interaction is intensified, leading to larger level splittings and thus an opening of the gap. This interpretation is corroborated by the fact that for these three systems according to Figure 3d a particularly large out-of-plane contraction is found.

It shall also be highlighted that interesting linear band crossings, i.e., Dirac-like points, are observed in the band structures of 2D $AgBiO_3$ and $BiNaO_3$ at the high-symmetry *K*-point (see Figures S13 and S14), warranting further

https://doi.org/10.1021/acs.nanolett.1c03841
Nano Lett. 2022, 22, 989−997

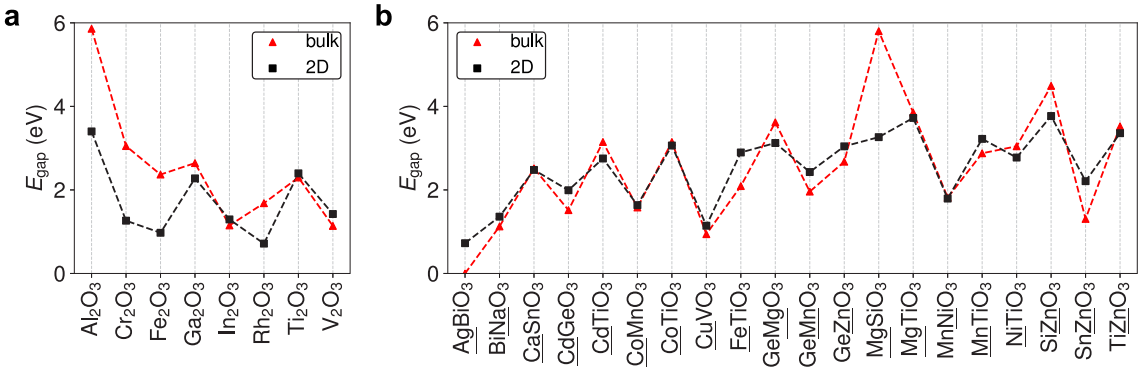

Figure 4. Band gap changes upon exfoliation. Comparison of the calculated band gaps of the bulk and 2D systems for the (a) binary and (b) ternary compounds.

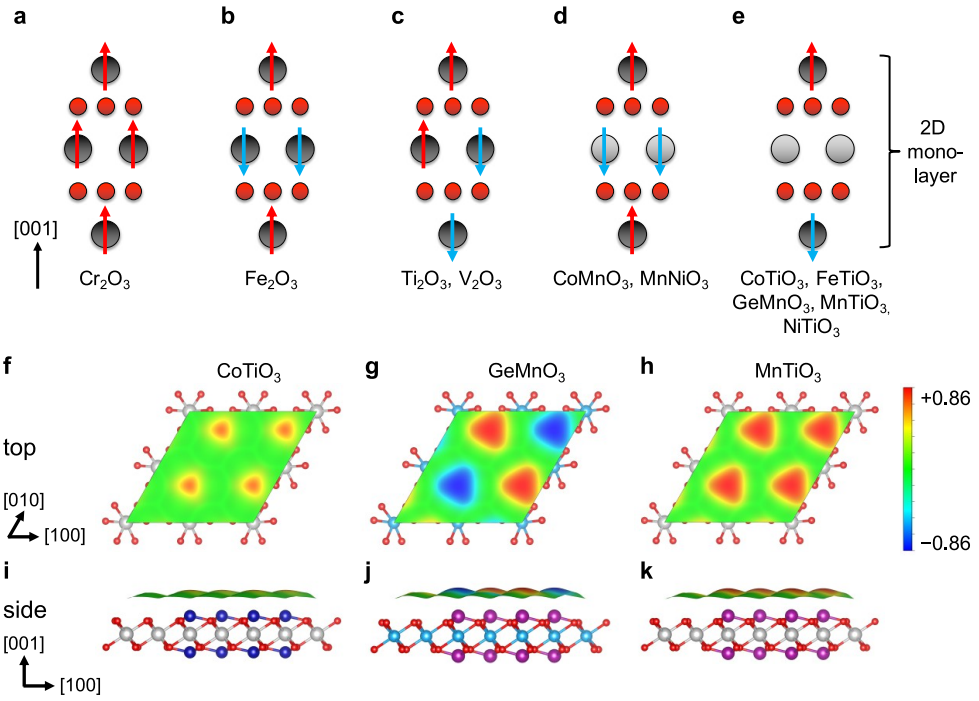

Figure 5. Magnetic configurations and surface spin polarizations. Schematic representation of the magnetic configurations for (a–c) binary and (d and e) ternary 2D systems. The compositions for which the specific configuration applies are indicated at the bottom. Cations are visualized by black and light gray spheres, whereas oxygen anions are in red. Surface spin polarization on an isosurface of the charge density for (f and i) $CoTiO_3$, (g and j) $GeMnO_3$, and (h and k) $MnTiO_3$ in the top and side views, respectively. The isovalue for the charge density is 3×10^{-4} $e/Å^3$. The scale bar indicates the degree of spin polarization. Colors: Co, dark blue; Ti, light gray; Ge, light blue; Mn, magenta; and O, red.

investigations on the potential topological nature of these systems and other non-vdW 2D materials.

MAGNETISM

These mainly transition metal based 2D systems are especially interesting in terms of their magnetic properties as already reported for hematene and ilmenene.[29,30] Table 1 also indicates for which of the bulk parent systems a finite magnetic moment is reported in the AFLOW database. Hence, 4 (7) of 8 (20) binary (ternary) systems are found to be magnetic. While the standard workflow[66] of AFLOW might be biased toward ferromagnetic (FM) configurations with small magnetic moments, we have further investigated the preferred magnetic ordering according to the algorithm developed within the coordination corrected enthalpies (CCE) method[67,68] (see Methods section for details). This ansatz reliably finds the antiferromagnetic (AFM) configurations of hematite and hematene reported previously.[40] Note that, for the 2D systems, the size of the surface moments (outer moments) is generally not equal to the ones within the slab (inner moments), and hence the AFM configuration might have a small net moment. This is particularly evident for ternary systems with two different magnetic ions such as $CoMnO_3$ and $MnNiO_3$.

The spin configurations found are indicated in Figure 5a–e, and additional results including the energy difference $\Delta E = E_{AFM} - E_{FM}$ between the lowest energy AFM and FM ordering and magnetic moments also including bulk reference data are summarized in Table 2. Results for SCAN are included in Section VI in the Supporting Information. The 2D materials are primarily AFM with the exception of Cr_2O_3, which becomes FM (Figure 5a) upon confinement to 2D as noted previously, albeit for oxygen terminated slabs.[46] For Fe_2O_3, the

https://doi.org/10.1021/acs.nanolett.1c03841
Nano Lett. 2022, 22, 989−997

Table 2. Magnetic Properties[a]

	mag. order type		ΔE			μ_{2D}			mag. order type		ΔE		μ_{bulk}		μ_{2D}	
formula	bulk	2D	bulk	2D	μ_{bulk}	inner	outer	formula	bulk	2D	bulk	2D	*A* el.	*B* el.	inner	outer
Cr_2O_3	AFM	FM	−0.044	0.013	2.91	2.97	3.04	$\underline{Co}MnO_3$	AFM	AFM	−0.024	−0.062	2.77	3.07	3.12	2.72
Fe_2O_3	AFM	AFM	−0.489	−0.479	4.18	4.20	4.01	$\underline{Co}TiO_3$	FM	AFM	0.004	−0.011	2.79	0.06	0.00	2.74
Ti_2O_3	AFM	AFM	−0.893	−0.094	0.87	0.89	0.74	$\underline{Fe}TiO_3$	FM	AFM	0.003	−0.007	3.72	0.08	0.00	3.69
V_2O_3	AFM	AFM	−0.013	−0.090	1.83	1.84	1.67	$GeMnO_3$	AFM	AFM	−0.041	−0.014	0.01	4.61	0.00	4.57
								$MnNiO_3$	AFM	AFM	−0.054	−0.147	3.07	1.73	3.13	1.69
								$\underline{Mn}TiO_3$	AFM	AFM	−0.027	−0.018	4.60	0.02	0.00	4.55
								$\underline{Ni}TiO_3$	FM	AFM	0.001	−0.001	1.75	0.07	0.00	1.73

[a]Energetically preferred magnetic ordering type, energy difference $\Delta E = E_{AFM} - E_{FM}$ between lowest energy AFM and FM ordering in eV/formula unit, and absolute magnetic moments for the inner and outer magnetic ions of the slab in μ_B for the bulk and corresponding [001] facets. For ternaries, the *A* element is the first cation species in the formula while the *B* element corresponds to the second. The terminating elements of the slabs (outer ions) are underlined.

moments of the inner ions are antialigned to the ones at the bottom and top, Figure 5b. On the contrary, for Ti_2O_3 and V_2O_3 also the inner moments show AFM ordering, resulting in the top and bottom moments being antialigned (Figure 5c). For ternaries, only two types of magnetic configurations are observed (Figures 5d,e). If two magnetic species are present as for $CoMnO_3$ and $MnNiO_3$, the inner moments are AFM to the outer ones. For the other cases with only one magnetic species, the spins at the top and bottom are AFM. The surface moments generally reduce by up to ∼0.2 μ_B when compared to their bulk references. The only exception is Cr_2O_3, for which they are slightly enhanced.

Even with most systems being AFM, the preferred termination of the 2D materials by the species in the lower oxidation state causes the magnetic ions of the ternary systems, i.e., Mn^{2+}, Fe^{2+}, Co^{2+}, and Ni^{2+}, to be at the surface. This outlines an ideal playground for spintronics since the spin polarization at surfaces can be accessed by techniques such as spin-polarized scanning tunneling microscopy (STM) and tuned by, e.g., adsorbates.[40,69] While the 2D systems themselves are found to be insulating, it has already been demonstrated that, due to weak interactions, the electronic and magnetic properties of hematene were well preserved on Au(111)[45]—a prototypical substrate in surface science.

To underscore this point, Figure 5f–k presents the surface spin polarization on an isosurface of the charge density for $CoTiO_3$, $GeMnO_3$, and $MnTiO_3$. We decided to use the total charge density to clearly indicate that the whole density is strongly spin-polarized and not just a part of it within a certain energy interval (as sampled by STM). For this, we have studied the FM and AFM alignment of the surface spins in a 2 × 2 supercell, as the interplane couplings (see Figure 5a–e) are regarded to be reliably determined from the study of the structural unit cell. For $GeMnO_3$, the surface moments couple antiferromagnetically, whereas for the other systems FM order is observed. As indicated in Figure 5, for $CoTiO_3$, a positive polarization reaching up to ∼70% in a narrow region above the Co centers is found. $GeMnO_3$ depicts a strong spatial variation of the polarization from −86% to +86% due to the AFM in-plane coupling. Finally, $MnTiO_3$ shows high positive values extending over a larger spatial range above the Mn ions compared to $CoTiO_3$, also reaching a maximum of +86%. These examples showcase the versatile degree of surface spin polarization that can be expected from non-vdW 2D materials offering great potential for spintronic applications.

CONCLUSIONS

We have outlined a new set of non-vdW 2D materials by employing data-driven concepts and extensive calculations. By filtering the AFLOW-ICSD database according to the structural prototype of the two first systems realized experimentally, we have obtained 8 binary and 20 ternary candidates. The oxidation number of the cations at the surface of the 2D slab is identified as a suitable descriptor for exfoliability, i.e., indicating easy exfoliation in the case of a low oxidation state—a principle of likely high value for future 2D materials discovery. In terms of the structure, the 2D systems show a strong vertical contraction and lateral expansion as compared to the bulk parents. The band gaps are distributed over a large range, and potential topological features are exhibited by several candidates. The magnetic properties are especially appealing: while most spin-polarized systems show AFM ordering, the magnetic ions are at the surface, which leads to a very diverse set of surface spin polarizations, foreshadowing potential applications in spintronics. Eventually, surface functionalization by appropriate molecular adsorbates can be a fruitful future direction to selectively enhance the properties of the outlined compounds. We thus anticipate that our study will prove useful for the discovery of new non-vdW 2D systems and will unravel the potential of this class of novel materials.

METHODS

The *ab initio* calculations for the exchange-correlation functionals LDA,[70,71] PBE,[72] SCAN,[73] and PBE+*U*[74−76] are performed with AFLOW[77,78] and the Vienna *Ab-initio* Simulation Package (VASP)[79−81] with settings according to the AFLOW standard[66] and the internal VASP precision set to ACCURATE. For calculations with SCAN, projector-augmented-wave (PAW) pseudopotentials[82] of VASP version 5.4 are used, and nonspherical contributions to the gradient of the density in the PAW spheres are explicitly included for SCAN and PBE+*U*. The [001] monolayer 2D facets are constructed from the bulk standard conventional unit cell with the respective AFLOW commands,[83] resulting in structures with 10 atoms, and at least 20 Å of vacuum perpendicular to the slabs are included. For the facets, both the ionic positions and the cell shape are allowed to relax unless stated otherwise. The AFLOW internal automatic determination of *k*-point sets is used, and for the calculations of the 2D facets, the setting for the number of *k*-points per reciprocal atom[66] is reduced to 1000, resulting in Γ-centered 10 × 10 × 1 grids.

https://doi.org/10.1021/acs.nanolett.1c03841
Nano Lett. 2022, 22, 989−997

The bulk and 2D candidate systems containing potentially magnetic elements such as Ti, V, Cr, Mn, Fe, Co, Ni, and Rh are rigorously checked for magnetism, using the algorithm developed within the CCE method,[67,68] i.e., investigating all possible FM and AFM configurations in the structural unit cell for five different sizes of induced magnetic moments each. The analysis is only applied to other systems when the standard workflow of AFLOW[66] resulted in finite magnetic moments after the relaxation. Ferrimagnetic configurations, i.e., having one moment antialigned to the other three in the unit cell, are only checked for the bulk binary systems but never resulted in the lowest energy configuration; hence, they are not considered for the 2D facets and ternary systems. In each case, the lowest energy magnetic state is used for the further calculations.

The exfoliation energy is computed as

$$\Delta E_{exf} = \frac{E_{slab} - E_{bulk}}{A} \quad (1)$$

where E_{slab} and E_{bulk} indicate the total energies of the relaxed 2D material and bulk, respectively, and A is the in-plane surface area according to the relaxed bulk unit cell. As pointed out in ref 59, the exfoliation energy from the surface of the material is exactly equal to the binding energy between layers/facets in the bulk.

The spin polarization is defined as

$$P = \frac{n_\uparrow - n_\downarrow}{n_\uparrow + n_\downarrow} \quad (2)$$

where $n_\uparrow$ and $n_\downarrow$ correspond to up spin and down spin densities, respectively. For the relaxed 2D systems, a static electronic calculation on 2 × 2 supercells was carried out. FM and AFM in-plane magnetic ordering was considered with the size of the magnetic moments induced according to the lowest energy magnetic configuration found for the structural unit cell. In each case, due to the weak in-plane magnetic coupling, the forces on the atoms and stress on the supercell were found to be negligibly small in each case.

Numerical data for the exfoliation energies, structural parameters, and magnetic properties are included in Section VI in the Supporting Information.

■ ASSOCIATED CONTENT

Supporting Information

The Supporting Information is available free of charge at https://pubs.acs.org/doi/10.1021/acs.nanolett.1c03841.

Exfoliation energies for additional functionals and from relaxing different degrees of freedom, exfoliation energies for different terminations for ternaries, change of structural parameters for SCAN, band structures for all binaries and ternaries, and tables with numerical data. (PDF)

■ AUTHOR INFORMATION

Corresponding Author

Rico Friedrich − *Institute of Ion Beam Physics and Materials Research, Helmholtz-Zentrum Dresden-Rossendorf, 01328 Dresden, Germany; Center for Autonomous Materials Design, Duke University, Durham, North Carolina 27708, United States;* orcid.org/0000-0002-4066-3840; Email: r.friedrich@hzdr.de

Authors

Mahdi Ghorbani-Asl − *Institute of Ion Beam Physics and Materials Research, Helmholtz-Zentrum Dresden-Rossendorf, 01328 Dresden, Germany;* orcid.org/0000-0003-3060-4369

Stefano Curtarolo − *Center for Autonomous Materials Design, Duke University, Durham, North Carolina 27708, United States; Materials Science, Electrical Engineering, and Physics, Duke University, Durham, North Carolina 27708, United States;* orcid.org/0000-0003-0570-8238

Arkady V. Krasheninnikov − *Institute of Ion Beam Physics and Materials Research, Helmholtz-Zentrum Dresden-Rossendorf, 01328 Dresden, Germany; Department of Applied Physics, Aalto University, Aalto 00076, Finland;* orcid.org/0000-0003-0074-7588

Complete contact information is available at: https://pubs.acs.org/10.1021/acs.nanolett.1c03841

Notes

The authors declare no competing financial interest.

■ ACKNOWLEDGMENTS

The authors thank the HZDR Computing Center, HLRS, Stuttgart, Germany, and TU Dresden Cluster "Taurus" for generous grants of CPU time. R.F. acknowledges support from the Alexander von Humboldt foundation under the Feodor Lynen research fellowship. A.V.K. thanks the German Research Foundation (DFG) for the support through Project KR 4866/2-1 and the collaborative research center "Chemistry of Synthetic 2D Materials" SFB-1415-417590517. R.F. thanks Marco Esters, Corey Oses, David Hicks, Silvan Kretschmer, and Xiomara Campilongo for fruitful discussions.

■ REFERENCES

(1) Novoselov, K. S.; Geim, A. K.; Morozov, S. V.; Jiang, D.; Zhang, Y.; Dubonos, S. V.; Grigorieva, I. V.; Firsov, A. A. Electric Field Effect in Atomically Thin Carbon Films. *Science* **2004**, *306*, 666−669.

(2) Cao, Y.; Fatemi, V.; Fang, S.; Watanabe, K.; Taniguchi, T.; Kaxiras, E.; Jarillo-Herrero, P. Unconventional superconductivity in magic-angle graphene superlattices. *Nature* **2018**, *556*, 43−50.

(3) Campi, D.; Kumari, S.; Marzari, N. Prediction of Phonon-Mediated Superconductivity with High Critical Temperature in the Two-Dimensional Topological Semimetal W_2N_3. *Nano Lett.* **2021**, *21*, 3435−3442.

(4) Butler, S. Z.; Hollen, S. M.; Cao, L.; Cui, Y.; Gupta, J. A.; Gutiérrez, H. R.; Heinz, T. F.; Hong, S. S.; Huang, J.; Ismach, A. F.; et al. Progress, Challenges, and Opportunities in Two-Dimensional Materials Beyond Graphene. *ACS Nano* **2013**, *7*, 2898−2926.

(5) Chhowalla, M.; Shin, H. S.; Eda, G.; Li, L.-J.; Loh, K. P.; Zhang, H. The chemistry of two-dimensional layered transition metal dichalcogenide nanosheets. *Nat. Chem.* **2013**, *5*, 263−275.

(6) Manzeli, S.; Ovchinnikov, D.; Pasquier, D.; Yazyev, O. V.; Kis, A. 2D transition metal dichalcogenides. *Nat. Rev. Mater.* **2017**, *2*, 17033.

(7) Burch, K. S.; Mandrus, D.; Park, J.-G. Magnetism in two-dimensional van der Waals materials. *Nature* **2018**, *563*, 47−52.

(8) Gibertini, M.; Koperski, M.; Morpurgo, A. F.; Novoselov, K. S. Magnetic 2D materials and heterostructures. *Nat. Nanotechnol.* **2019**, *14*, 408−419.

(9) Huang, Y. L.; Chen, W.; Wee, A. T. S. Two-dimensional magnetic transition metal chalcogenides. *SmartMat* **2021**, *2*, 139−153.

(10) Kou, L.; Ma, Y.; Sun, Z.; Heine, T.; Chen, C. Two-Dimensional Topological Insulators: Progress and Prospects. *J. Phys. Chem. Lett.* **2017**, *8*, 1905−1919.

(11) Wang, Q. H.; Kalantar-Zadeh, K.; Kis, A.; Coleman, J. N.; Strano, M. S. Electronics and optoelectronics of two-dimensional transition metal dichalcogenides. *Nat. Nanotechnol.* **2012**, *7*, 699−712.
(12) Lemme, M. C.; Li, L.-J.; Palacios, T.; Schwierz, F. Two-dimensional materials for electronic applications. *MRS Bull.* **2014**, *39*, 711−718.
(13) Deng, D.; Novoselov, K. S.; Fu, Q.; Zheng, N.; Tian, Z.; Bao, X. Catalysis with two-dimensional materials and their heterostructures. *Nat. Nanotechnol.* **2016**, *11*, 218−230.
(14) Wang, Y.; Mao, J.; Meng, X.; Yu, L.; Deng, D.; Bao, X. Catalysis with Two-Dimensional Materials Confining Single Atoms: Concept, Design, and Applications. *Chem. Rev.* **2019**, *119*, 1806−1854.
(15) Anasori, B.; Lukatskaya, M. R.; Gogotsi, Y. 2D metal carbides and nitrides (MXenes) for energy storage. *Nat. Rev. Mater.* **2017**, *2*, 16098.
(16) Wang, J.; Malgras, V.; Sugahara, Y.; Yamauchi, Y. Electrochemical energy storage performance of 2D nanoarchitectured hybrid materials. *Nat. Commun.* **2021**, *12*, 3563.
(17) Chepkasov, I. V.; Ghorbani-Asl, M.; Popov, Z. I.; Smet, J. H.; Krasheninnikov, A. V. Alkali metals inside bi-layer graphene and MoS_2: Insights from first-principles calculations. *Nano Energy* **2020**, *75*, 104927.
(18) Novoselov, K. S.; Jiang, D.; Schedin, F.; Booth, T. J.; Khotkevich, V. V.; Morozov, S. V.; Geim, A. K. Two-dimensional atomic crystals. *Proc. Natl. Acad. Sci. U. S. A.* **2005**, *102*, 10451−10453.
(19) Nicolosi, V.; Chhowalla, M.; Kanatzidis, M. G.; Strano, M. S.; Coleman, J. N. Liquid Exfoliation of Layered Materials. *Science* **2013**, *340*, 1226419.
(20) Penev, E. S.; Marzari, N.; Yakobson, B. I. Theoretical Prediction of Two-Dimensional Materials, Behavior, and Properties. *ACS Nano* **2021**, *15*, 5959−5976.
(21) Lebègue, S.; Björkman, T.; Klintenberg, M.; Nieminen, R. M.; Eriksson, O. Two-Dimensional Materials from Data Filtering and Ab Initio Calculations. *Phys. Rev. X* **2013**, *3*, 031002.
(22) Rasmussen, F. A.; Thygesen, K. S. Computational 2D Materials Database: Electronic Structure of Transition-Metal Dichalcogenides and Oxides. *J. Phys. Chem. C* **2015**, *119*, 13169−13183.
(23) Choudhary, K.; Kalish, I.; Beams, R.; Tavazza, F. High-throughput Identification and Characterization of Two-dimensional Materials using Density functional theory. *Sci. Rep.* **2017**, *7*, 5179.
(24) Cheon, G.; Duerloo, K.-A. N.; Sendek, A. D.; Porter, C.; Chen, Y.; Reed, E. J. Data Mining for New Two- and One-Dimensional Weakly Bonded Solids and Lattice-Commensurate Heterostructures. *Nano Lett.* **2017**, *17*, 1915−1923.
(25) Mounet, N.; Gibertini, M.; Schwaller, P.; Campi, D.; Merkys, A.; Marrazzo, A.; Sohier, T.; Castelli, I. E.; Cepellotti, A.; Pizzi, G.; et al. Two-dimensional materials from high-throughput computational exfoliation of experimentally known compounds. *Nat. Nanotechnol.* **2018**, *13*, 246−252.
(26) Besse, R.; Lima, M. P.; Da Silva, J. L. F. First-Principles Exploration of Two-Dimensional Transition Metal Dichalcogenides Based on Fe, Co, Ni, and Cu Groups and Their van der Waals Heterostructures. *ACS Appl. Energy Mater.* **2019**, *2*, 8491−8501.
(27) Núñez, M.; Weht, R.; Núñez-Regueiro, M. Searching for electronically two dimensional metals in high-throughput ab initio databases. *Comput. Mater. Sci.* **2020**, *182*, 109747.
(28) Schleder, G. R.; Acosta, C. M.; Fazzio, A. Exploring Two-Dimensional Materials Thermodynamic Stability via Machine Learning. *ACS Appl. Mater. Interfaces* **2020**, *12*, 20149−20157.
(29) Puthirath Balan, A.; Radhakrishnan, S.; Woellner, C. F.; Sinha, S. K.; Deng, L.; Reyes, C. d. l.; Rao, B. M.; Paulose, M.; Neupane, R.; Apte, A.; et al. Exfoliation of a non-van der Waals material from iron ore hematite. *Nat. Nanotechnol.* **2018**, *13*, 602−609.
(30) Puthirath Balan, A.; Radhakrishnan, S.; Kumar, R.; Neupane, R.; Sinha, S. K.; Deng, L.; de los Reyes, C. A.; Apte, A.; Rao, B. M.; Paulose, M.; et al. A Non-van der Waals Two-Dimensional Material from Natural Titanium Mineral Ore Ilmenite. *Chem. Mater.* **2018**, *30*, 5923−5931.
(31) Yadav, T. P.; Shirodkar, S. N.; Lertcumfu, N.; Radhakrishnan, S.; Sayed, F. N.; Malviya, K. D.; Costin, G.; Vajtai, R.; Yakobson, B. I.; Tiwary, C. S.; et al. Chromiteen: A New 2D Oxide Magnetic Material from Natural Ore. *Adv. Mater. Interfaces* **2018**, *5*, 1800549.
(32) Puthirath, A. B.; Shirodkar, S. N.; Gao, G.; Hernandez, F. C. R.; Deng, L.; Dahal, R.; Apte, A.; Costin, G.; Chakingal, N.; Balan, A. P.; et al. Scale-Enhanced Magnetism in Exfoliated Atomically Thin Magnetite Sheets. *Small* **2020**, *16*, 2004208.
(33) Kaur, H.; Tian, R.; Roy, A.; McCrystall, M.; Horvath, D. V.; Lozano Onrubia, G.; Smith, R.; Ruether, M.; Griffin, A.; Backes, C.; et al. Production of Quasi-2D Platelets of Nonlayered Iron Pyrite (FeS_2) by Liquid-Phase Exfoliation for High Performance Battery Electrodes. *ACS Nano* **2020**, *14*, 13418−13432.
(34) Puthirath, A. B.; Balan, A. P.; Oliveira, E. F.; Sreepal, V.; Robles Hernandez, F. C.; Gao, G.; Chakingal, N.; Sassi, L. M.; Thibeorchews, P.; Costin, G.; et al. Apparent Ferromagnetism in Exfoliated Ultrathin Pyrite Sheets. *J. Phys. Chem. C* **2021**, *125*, 18927−18935.
(35) Moinuddin, M. G.; Srinivasan, S.; Sharma, S. K. Probing Ferrimagnetic Semiconductor with Enhanced Negative Magnetoresistance: 2D Chromium Sulfide. *Adv. Electron. Mater.* **2021**, *7*, 2001116.
(36) Hu, L.; Cao, L.; Li, L.; Duan, J.; Liao, X.; Long, F.; Zhou, J.; Xiao, Y.; Zeng, Y.-J.; Zhou, S. Two-dimensional magneto-photoconductivity in non-van der Waals manganese selenide. *Mater. Horiz.* **2021**, *8*, 1286−1296.
(37) Yousaf, A.; Gilliam, M. S.; Chang, S. L. Y.; Augustin, M.; Guo, Y.; Tahir, F.; Wang, M.; Schwindt, A.; Chu, X. S.; Li, D. O.; et al. Exfoliation of Quasi-Two-Dimensional Nanosheets of Metal Diborides. *J. Phys. Chem. C* **2021**, *125*, 6787−6799.
(38) Guo, Y.; Gupta, A.; Gilliam, M. S.; Debnath, A.; Yousaf, A.; Saha, S.; Levin, M. D.; Green, A. A.; Singh, A. K.; Wang, Q. H. Exfoliation of boron carbide into ultrathin nanosheets. *Nanoscale* **2021**, *13*, 1652−1662.
(39) Gibaja, C.; Rodríguez-San-Miguel, D.; Paz, W. S.; Torres, I.; Salagre, E.; Segovia, P.; Michel, E. G.; Assebban, M.; Ares, P.; Hernández-Maldonado, D.; et al. Exfoliation of Alpha-Germanium: A Covalent Diamond-Like Structure. *Adv. Mater.* **2021**, *33*, 2006826.
(40) Wei, Y.; Ghorbani-Asl, M.; Krasheninnikov, A. V. Tailoring the Electronic and Magnetic Properties of Hematene by Surface Passivation: Insights from First-Principles Calculations. *J. Phys. Chem. C* **2020**, *124*, 22784−22792.
(41) Zhang, B. Y.; Xu, K.; Yao, Q.; Jannat, A.; Ren, G.; Field, M. R.; Wen, X.; Zhou, C.; Zavabeti, A.; Ou, J. Z. Hexagonal metal oxide monolayers derived from the metal−gas interface. *Nat. Mater.* **2021**, *20*, 1073−1078.
(42) Wei, Y.; Liu, C.; Wang, T.; Zhang, Y.; Qi, C.; Li, H.; Ma, G.; Liu, Y.; Dong, S.; Huo, M. Electronegativity regulation on optelectronic properties of non van der Waals two-dimensional material: Ga_2O_3. *Comput. Mater. Sci.* **2020**, *179*, 109692.
(43) Jin, C.; Kou, L. Two-dimensional non-van der Waals magnetic layers: functional materials for potential device applications. *J. Phys. D: Appl. Phys.* **2021**, *54*, 413001.
(44) Padilha, A. C. M.; Soares, M.; Leite, E. R.; Fazzio, A. Theoretical and Experimental Investigation of 2D Hematite. *J. Phys. Chem. C* **2019**, *123*, 16359−16365.
(45) Gonzalez, R. I.; Mella, J.; Díaz, P.; Allende, S.; Vogel, E. E.; Cardenas, C.; Munoz, F. Hematene: a 2D magnetic material in van der Waals or non-van der Waals heterostructures. *2D Mater.* **2019**, *6*, 045002.
(46) Bandyopadhyay, A.; Frey, N. C.; Jariwala, D.; Shenoy, V. B. Engineering Magnetic Phases in Two-Dimensional Non-van der Waals Transition-Metal Oxides. *Nano Lett.* **2019**, *19*, 7793−7800.
(47) Chahal, S.; Kauzlarich, S. M.; Kumar, P. Microwave Synthesis of Hematene and Other Two-Dimensional Oxides. *ACS Materials Lett.* **2021**, *3*, 631−640.
(48) Mohapatra, J.; Ramos, A.; Elkins, J.; Beatty, J.; Xing, M.; Singh, D.; La Plante, E. C.; Ping Liu, J. Ferromagnetism in 2D α-Fe_2O_3 nanosheets. *Appl. Phys. Lett.* **2021**, *118*, 183102.

https://doi.org/10.1021/acs.nanolett.1c03841
Nano Lett. 2022, 22, 989−997

(49) Momma, K.; Izumi, F. *VESTA3* for three-dimensional visualization of crystal, volumetric and morphology data. *J. Appl. Crystallogr.* **2011**, *44*, 1272−1276.
(50) Liu, S.; Xie, L.; Qian, H.; Liu, G.; Zhong, H.; Zeng, H. Facile preparation of novel and active 2D nanosheets from non-layered and traditionally non-exfoliable earth-abundant materials. *J. Mater. Chem. A* **2019**, *7*, 15411−15419.
(51) Curtarolo, S.; Setyawan, W.; Wang, S.; Xue, J.; Yang, K.; Taylor, R. H.; Nelson, L. J.; Hart, G. L. W.; Sanvito, S.; Buongiorno Nardelli, M.; et al. AFLOWLIB.ORG: A distributed materials properties repository from high-throughput *ab initio* calculations. *Comput. Mater. Sci.* **2012**, *58*, 227−235.
(52) Hicks, D.; Oses, C.; Gossett, E.; Gomez, G.; Taylor, R. H.; Toher, C.; Mehl, M. J.; Levy, O.; Curtarolo, S. *AFLOW-SYM*: platform for the complete, automatic and self-consistent symmetry analysis of crystals. *Acta Crystallogr., Sect. A* **2018**, *74*, 184−203.
(53) Hicks, D.; Toher, C.; Ford, D. C.; Rose, F.; De Santo, C.; Levy, O.; Mehl, M. J.; Curtarolo, S. AFLOW-XtalFinder: a reliable choice to identify crystalline prototypes. *npj Comput. Mater.* **2021**, *7*, 30.
(54) Taylor, R. H.; Rose, F.; Toher, C.; Levy, O.; Yang, K.; Buongiorno Nardelli, M.; Curtarolo, S. A RESTful API for exchanging materials data in the AFLOWLIB.org consortium. *Comput. Mater. Sci.* **2014**, *93*, 178−192.
(55) Rose, F.; Toher, C.; Gossett, E.; Oses, C.; Buongiorno Nardelli, M.; Fornari, M.; Curtarolo, S. AFLUX: The LUX materials search API for the AFLOW data repositories. *Comput. Mater. Sci.* **2017**, *137*, 362−370.
(56) Mehl, M. J.; Hicks, D.; Toher, C.; Levy, O.; Hanson, R. M.; Hart, G. L. W.; Curtarolo, S. The AFLOW Library of Crystallographic Prototypes: Part 1. *Comput. Mater. Sci.* **2017**, *136*, S1−S828.
(57) Backes, C.; Campi, D.; Szydlowska, B. M.; Synnatschke, K.; Ojala, E.; Rashvand, F.; Harvey, A.; Griffin, A.; Sofer, Z.; Marzari, N.; et al. Equipartition of Energy Defines the Size−Thickness Relationship in Liquid-Exfoliated Nanosheets. *ACS Nano* **2019**, *13*, 7050−7061.
(58) Zacharia, R.; Ulbricht, H.; Hertel, T. Interlayer cohesive energy of graphite from thermal desorption of polyaromatic hydrocarbons. *Phys. Rev. B* **2004**, *69*, 155406.
(59) Jung, J. H.; Park, C.-H.; Ihm, J. A Rigorous Method of Calculating Exfoliation Energies from First Principles. *Nano Lett.* **2018**, *18*, 2759−2765.
(60) Sun, J.; Remsing, R. C.; Zhang, Y.; Sun, Z.; Ruzsinszky, A.; Peng, H.; Yang, Z.; Paul, A.; Waghmare, U.; Wu, X.; et al. Accurate first-principles structures and energies of diversely bonded systems from an efficient density functional. *Nat. Chem.* **2016**, *8*, 831.
(61) Mohanty, B.; Wei, Y.; Ghorbani-Asl, M.; Krasheninnikov, A. V.; Rajput, P.; Jena, B. K. Revealing the defect-dominated oxygen evolution activity of hematene. *J. Mater. Chem. A* **2020**, *8*, 6709−6716.
(62) Navrotsky, A.; Ma, C.; Lilova, K.; Birkner, N. Nanophase Transition Metal Oxides Show Large Thermodynamically Driven Shifts in Oxidation-Reduction Equilibria. *Science* **2010**, *330*, 199−201.
(63) Kvashnin, A. G.; Kvashnin, D. G.; Oganov, A. R. Novel Unexpected Reconstructions of (100) and (111) Surfaces of NaCl: Theoretical Prediction. *Sci. Rep.* **2019**, *9*, 14267.
(64) Bahn, S. R.; Jacobsen, K. W. An object-oriented scripting interface to a legacy electronic structure code. *Comput. Sci. Eng.* **2002**, *4*, 56−66.
(65) Hjorth Larsen, A.; Jørgen Mortensen, J. J.; Blomqvist, J.; Castelli, I. E.; Christensen, R.; Dułak, M.; Friis, J.; Groves, M. N.; Hammer, B.; Hargus, C.; et al. The atomic simulation environment—a Python library for working with atoms. *J. Phys.: Condens. Matter* **2017**, *29*, 273002.
(66) Calderon, C. E.; Plata, J. J.; Toher, C.; Oses, C.; Levy, O.; Fornari, M.; Natan, A.; Mehl, M. J.; Hart, G. L. W.; Buongiorno Nardelli, M.; et al. The AFLOW standard for high-throughput materials science calculations. *Comput. Mater. Sci.* **2015**, *108*, 233−238.
(67) Friedrich, R.; Usanmaz, D.; Oses, C.; Supka, A.; Fornari, M.; Buongiorno Nardelli, M.; Toher, C.; Curtarolo, S. Coordination corrected ab initio formation enthalpies. *npj Comput. Mater.* **2019**, *5*, 59.
(68) Friedrich, R.; Esters, M.; Oses, C.; Ki, S.; Brenner, M. J.; Hicks, D.; Mehl, M. J.; Toher, C.; Curtarolo, S. Automated coordination corrected enthalpies with AFLOW-CCE. *Phys. Rev. Mater.* **2021**, *5*, 043803.
(69) Heß, V.; Friedrich, R.; Matthes, F.; Caciuc, V.; Atodiresei, N.; Bürgler, D. E.; Blügel, S.; Schneider, C. M. Magnetic subunits within a single molecule−surface hybrid. *New J. Phys.* **2017**, *19*, 053016.
(70) Kohn, W.; Sham, L. J. Self-consistent equations including exchange and correlation effects. *Phys. Rev.* **1965**, *140*, A1133.
(71) von Barth, U.; Hedin, L. A local exchange-correlation potential for the spin polarized case: I. *J. Phys. C: Solid State Phys.* **1972**, *5*, 1629.
(72) Perdew, J. P.; Burke, K.; Ernzerhof, M. Generalized Gradient Approximation Made Simple. *Phys. Rev. Lett.* **1996**, *77*, 3865−3868.
(73) Sun, J.; Ruzsinszky, A.; Perdew, J. P. Strongly Constrained and Appropriately Normed Semilocal Density Functional. *Phys. Rev. Lett.* **2015**, *115*, 036402.
(74) Dudarev, S. L.; Botton, G. A.; Savrasov, S. Y.; Humphreys, C. J.; Sutton, A. P. Electron-energy-loss spectra and the structural stability of nickel oxide: An LSDA + *U* study. *Phys. Rev. B* **1998**, *57*, 1505−1509.
(75) Liechtenstein, A. I.; Anisimov, V. I.; Zaanen, J. Density-functional theory and strong interactions: Orbital ordering in Mott-Hubbard insulators. *Phys. Rev. B* **1995**, *52*, R5467−R5470.
(76) Anisimov, V. I.; Zaanen, J.; Andersen, O. K. Band theory and Mott insulators: Hubbard *U* instead of Stoner *I*. *Phys. Rev. B* **1991**, *44*, 943−954.
(77) Levy, O.; Chepulskii, R. V.; Hart, G. L. W.; Curtarolo, S. The New Face of Rhodium Alloys: Revealing Ordered Structures from First Principles. *J. Am. Chem. Soc.* **2010**, *132*, 833−837.
(78) Curtarolo, S.; Setyawan, W.; Hart, G. L. W.; Jahnátek, M.; Chepulskii, R. V.; Taylor, R. H.; Wang, S.; Xue, J.; Yang, K.; Levy, O.; et al. AFLOW: An automatic framework for high-throughput materials discovery. *Comput. Mater. Sci.* **2012**, *58*, 218−226.
(79) Kresse, G.; Hafner, J. *Ab initio* molecular dynamics for liquid metals. *Phys. Rev. B* **1993**, *47*, 558−561.
(80) Kresse, G.; Furthmüller, J. Efficient iterative schemes for *ab initio* total-energy calculations using a plane-wave basis set. *Phys. Rev. B* **1996**, *54*, 11169−11186.
(81) Kresse, G.; Furthmüller, J. Efficiency of *ab-initio* total energy calculations for metals and semiconductors using a plane-wave basis set. *Comput. Mater. Sci.* **1996**, *6*, 15−50.
(82) Kresse, G.; Joubert, D. From ultrasoft pseudopotentials to the projector augmented-wave method. *Phys. Rev. B* **1999**, *59*, 1758−1775.
(83) Chepulskii, R. V.; Curtarolo, S. First principles study of Ag, Au, and Cu surface segregation in FePt-$L1_0$. *Appl. Phys. Lett.* **2010**, *97*, 221908.

https://doi.org/10.1021/acs.nanolett.1c03841
Nano Lett. 2022, 22, 989−997